Tape-casting and freeze-drying gadolinia-doped ceria composite membranes for carbon dioxide permeation

S.G.M. Carvalho[a*], E.N.S. Muccillo[a], F.C. Fonseca[a], M. Müller[b], F. Schulze-Küppers[b], S. Baumann[b], W.A. Meulenberg[b], O. Guillon[b], R. Muccillo[a]

[a] Energy and Nuclear Research Institute, IPEN-CNEN, S. Paulo, SP, Brazil

[b] Institute of Energy and Climate Research, Forschungszentrum Jülich, Germany

Abstract

Porous ceria: 20 mol% gadolinia (20GDC) ceramic membranes were prepared by tape casting (TC) and freeze-drying (FD) techniques, obtaining ceramic matrices with randomly dispersed round pores and with an aligned pore structure, respectively. Samples were sintered at 1450 ºC, followed by infiltration of molten eutectic sodium-lithium carbonates (NLC). The pore morphology of 20GDC-TC and 20GDC-FD composite membranes was evaluated by analysis of scanning electron microscopy images. The electrical resistivity was determined by electrochemical impedance spectroscopy in the 1 Hz - 10 MHz frequency range from 300 ºC to 700 ºC, covering the solid-to-molten NLC temperature range, showing that the aligned pore structure improved the conductivity of the ceramic matrix in addition to facilitating molten carbonate infiltration, improving the total (bulk + interfaces) electrical conductivity of the composite membrane. Permeation experiments showed high CO_2 permeation rates reached 5.35 x 10^{-7} mol m^{-2} s^{-1} Pa^{-1} at 800 ºC. The infiltration of molten sodium-lithium carbonate in gadolinium-doped ceria prepared by the freeze-drying technique is proposed as an optimized procedure for producing membranes for carbon dioxide separation.

Keywords: porous gadolinia-doped ceria; molten sodium-lithium carbonates; composite membranes; carbon dioxide separation.

*Corresponding author: S.G.M. Carvalho, sabrina.carvalho@alumni.usp.br.

1. Introduction

The global economy is facing a major challenge related to the use of natural resources, mainly the use and exploration of fossil fuels [1]. There is growing consensus that the climate of the planet is changing, in close relation with the emission of greenhouse gases. Intense combustion of fossil fuels during the XX century has considerably increased the CO_2 concentration in the atmosphere. Such an increase is the main reason for the unprecedented rise in the average temperature of the Earth [1,2].

Currently, a variety of technologies are evaluated for their ability to capture CO_2 from power plant flue gas or other CO_2 intensive industries. The most commercial-ready technology (amine-based) is costly, energy intensive, and less attractive from an environmental point of view [3,4]. Membranes have a significant opportunity to be a low-cost and low-energy solution for flue gas CO_2 capture [5]. Most CO_2 separation membrane development is focused on porous polymer and inorganic structures that show adequate performance below 200 ^oC. At higher temperatures, their selectivity for CO_2 decreases [6,7].

Envisaging energy conservation, it is highly desirable to separate CO_2 from flue gas at the high temperature the gas is released. In addition, the possibility of a separation process performed by a membrane at elevated temperatures means that the permeated CO_2 could be used as raw material in other reactions, such as dry reforming of methane and reverse water-gas shift reaction, producing syngas [8-10].

For use in flue gas separation, the membrane must be chemically and thermally stable. One class of membrane with potential to offer this combination is the supported molten-salt membrane. This membrane for carbon dioxide permeation consists of a molten carbonate phase held within the porous structure of an inorganic solid [11]. Initially, metals were used as supports [12], with functional ceramics investigated later [13,14].

The dense dual-phase ceramic-carbonate membrane is composed of a porous solid oxygen ion-conductor ceramic support, infiltrated with molten carbonates (Figure 1a). The driving force for permeation is the difference between the partial pressure of CO_2 on each side of the membrane. The separation mechanism is based on the surface reaction between a gas-phase CO_2 from the feed side and oxygen ions from the ceramic phase to form CO_3^{2-}. The carbonate ion is transported

through the molten carbonate phase to the opposite side of the membrane where the reverse reaction occurs, releasing CO_2 on the permeated side of the membrane. This reaction also releases oxygen ions in the reverse path through the ceramic phase, to the feed side of the membrane, to start the reaction again [11,15].

Regarding the electrical behavior of the membrane and its transport mechanism, the two phases of the membrane can be viewed as parallel double cells with ionic resistors R and associated cell thermodynamic voltages V_o [16] (Figure 1b). Since there is no electric current flowing outside the electrochemical cells, the formal parallel cell arrangement in fact originates from a series-type association. For CO_2 to be transported through the membrane, the flow of carbonate ions needs to be balanced by a counter flow of O^{2-} ions. If one of the electrical resistances in this circuit is higher than the other, the membrane efficiency will be limited by the most resistive component, i.e., by the ceramic phase.

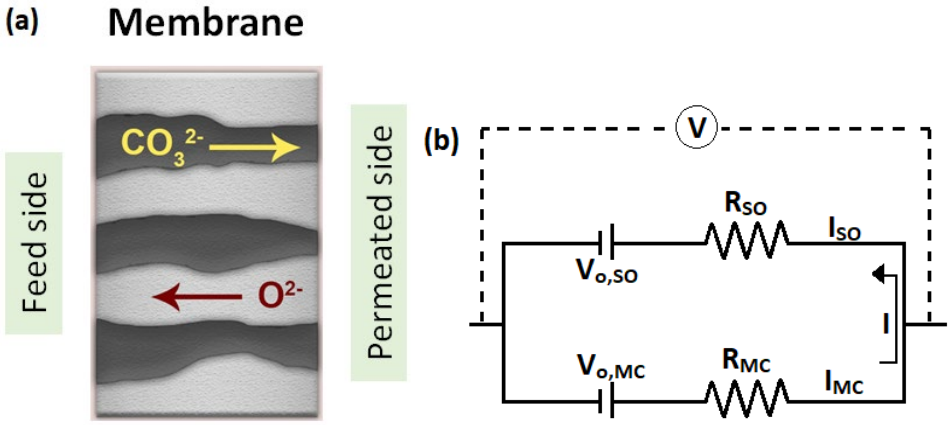

Figure 1–(a) Schematic illustration of ceramic-carbonate dual phase membrane for CO_2 separation, and (b) simplified electric circuit representing the composite membrane, adapted from [16]. SO and MC stand for solid oxide and molten carbonate, respectively.

Recently, many research groups are seeking to improve the efficiency of the membrane using different approaches, such as modifying the oxide ion ceramic support [17-21], studying the carbonate distribution [22] or composition [23,24] to be infiltrated in the ceramic matrix, or optimizing the membrane structure either by modifying its configuration [25] or by improving the pore structure of the ceramic phase [26].

The optimization of the pore structure of the membrane is an interesting

alternative to improve the membrane efficiency, as it may provide a decrease of the tortuosity and an enhancement of the carbon dioxide ion percolation inside the pores; this approach could lead to increasing membrane performance [27]. A simple technique for producing aligned pore structure is freeze casting; this technique consists in preparing an aqueous solution and a solid phase, which will be solidified, forming solid walls of solvent due to the repulsion of particles by the solidified fluid [28]. The porous structure is built after sublimation of the solidified fluid; a pore morphology is then produced, nearly consisting in a replica of the solidified (frozen) fluid pattern. Volume fraction, size, shape, and orientation of the porosity template can be controlled by both modifying the suspension characteristics and/or the solidification conditions, being possible to obtain an aligned pore structure (anisotropic freeze-casting) in a ceramic matrix.

This study is focused on the characterization of composite ceramic membranes produced by two techniques**:** i) tape casting of thin composite ceramic-carbonate membranes with a pore former to obtain randomly dispersed round pores**;** ii) freeze-drying [28-31], the porous ceramic matrix being produced by rapidly freezing its water-based suspension, producing an aligned pore structure, decreasing tortuosity [32] and improving the total electrical conductivity.

2. Experimental

2.1 Porous ceramic preparation

CeO_2: 20 mol% Gd_2O_3 (20GDC) (Ceramic Powder Technology AS, Norway) was used to prepare the porous ceramic membranes according to two techniques: tape casting (TC) and freeze drying (FD). For TC, 20GDC powder (20 vol.%) and rice starch (Remy Ind., Belgium), used as pore former with 10 wt.% in relation to the ceramic powder mass, were dispersed in a mixture (80 vol.%) of ethanol and methyl ethyl ketone with Tego Dispers 655 (Evonik Ind. AG, Germany) as a dispersant agent with 1.5 wt.% in relation to the ceramic powder mass. Polyvinyl butyral (Butvar PVB B-98, Solutia Inc., USA) was added as binder and Solusolv 2075 (Solutia Inc., USA) and PEG400 (polyethylene glycol 400, Merck KGaA, Germany) as plasticizers, with 7, 6 and 7 wt.% in relation to the ceramic powder mass, respectively. The prepared slurry was cast on a polymeric carrier foil by the doctor blade process with a casting

gap of 1.5 mm. After drying, the specimens were cut out from the green tape, debindered, and subsequently sintered in air at 1450 ^{o}C for 5 h.

For the preparation of porous supports with the freeze-drying technique, a water-based suspension containing 20GDC ceramic powder (25 vol.%), PEG4000S (Clariant, Switzerland) binder and Dolapix C64 (Zschimmer & Schwarz GmbH & Co, Germany) dispersant with 2.5 and 2.0 wt.% in relation to the ceramic powder mass**,** was prepared and mixed in a planetary mixer for blending and homogenization. The slurry was cast into a cylindrical mold with 80 mm height copper cylinder, followed by cooling in liquid nitrogen and drying inside a Martin Christ Epsilon 2-4 lyophilizer for over 15 h under low pressure. The green freeze-dried samples were sintered in air at 1450 ^{o}C for 5 h.

2.2 Molten carbonate Infiltration

A eutectic mixture of sodium and lithium carbonates (99.99%, Alfa Aesar, USA) was prepared by mixing the powders with 48 mol% Na_2CO_3 and 52 mol% Li_2CO_3. To achieve the infiltration of the molten carbonate into the sample, the porous ceramic was suspended by alumina holders. The eutectic carbonate mixture was slightly compacted, positioned on top of the porous ceramic membrane and placed inside a gas-tight furnace. Infiltration was carried out by heating the system at 600 ^{o}C during 1 h under CO_2 atmosphere. After the infiltration process, the samples were slightly sanded to remove the excess of solidified carbonate that had been accumulated on their surfaces.

2.3 Membrane characterization

The porosity and apparent density were evaluated by the Archimedes method based on the international standards ASTM C373-88, using water as liquid medium. The microstructure of both the porous and the composite (after infiltration) membranes were analyzed in scanning electron microscopes (Ultra55, Carl Zeiss NTS GmbH, Oberkochen, Germany and Inspect F50 FEG-SEM, FEI, Brno, Czech Republic).

The electrical properties of all samples were evaluated by electrochemical impedance spectroscopy. Measurements were carried out in the 300-700 ^{o}C range with a Solartron SI 1260 Impedance/Gain-phase Analyzer in the 1 Hz to 10 MHz frequency range with 200 mV AC amplitude; the impedance diagrams were analyzed with the ZView® software (Scribner Associates Inc.).

Permeation measurements were performed in an alumina membrane reactor. The membranes were fixed in an alumina tube of 12 mm inner diameter with a ceramic paste consisting of aluminum oxide, calcium oxide and titanium dioxide (Ceramacast Typ 510, Kager GmbH, Germany). Due to the constraint that CO must not be used in the laboratory and H_2 is limited to 2,9%, instead of synthesis gas, the gas used as feed was a mixture of CO_2 (20 vol.%), H_2O (15 vol.%), Ar (62.4 vol.%) and H_2 (2.6 vol.%) with a total flow rate of 200 mL min^{-1}, while a mixture of N_2 (97 vol.%) and water vapor (3 vol.%) at the same flow rate was used as a sweep gas. The permeated gas was analyzed with a mass spectrometer (Extrel, MAX300-EGA), monitoring Ar, CO_2, H_2, N_2 and H_2O. Effective sealing was confirmed by measuring the argon content on the permeate stream.

To evaluate the flux (J) of CO_2 through the membrane, the fractions (X) of CO_2 and Ar detected on the permeate side by the spectrometer, together with the total flow of carrier gas (f) and the active membrane area (S = 1.13 cm^2), were used in the following equations:

$$J_{CO_2 total} = \frac{X_{CO_2} \cdot f}{S}$$

$$J_{CO_2 leak} = \frac{R \cdot X_{Ar} \cdot f}{S}$$

$$J_{CO_2\ permeated} = J_{CO_2 total} - J_{CO_2 leak}$$

R is 0.25 and stands for the ratio between CO_2 and Ar detected both on the feed side. There was modification in the argon leakage upon temperature variation during the experiment, but it remained below 0.3% and 2% during heating and cooling, respectively. In addition to the CO_2 flux, permeance was evaluated by dividing the flux by the carbon dioxide partial pressure driving force; moreover, the permeability value was calculated by multiplying the permeance by the membrane thickness.

The ceramic paste used to fix the membrane to the alumina tube was analyzed after the permeation test by X-ray diffractometry (D8 Advance, Bruker-AXS, Karlsruhe, Germany) looking for the possible reason for the gas leak.

3. Results and Discussion

Both tape cast and freeze-dried samples exhibited 47 vol.% of porosity as evaluated by both the Archimedes method and the SEM image analysis. The average pore diameter for TC samples was evaluated as 3.4 μm, analyzed by SEM images using Image J software [33]. For FD samples, the average diameter of the cylindrical pore structure is 3.3 μm and, for both samples, 75% of the pores are below 4 μm. The skeletal density value (solid part + closed pores) of the ceramic phase of both TC and FD samples was calculated as 7.10 g cm^{-3}, which corresponds to 98% of the theoretical density of GDC. Despite similar values of both density and porosity, the pore structure of TC and FD samples was significantly different. Figure 2 shows SEM micrographs of samples produced by tape casting with rice starch as pore former, and by freeze-drying.

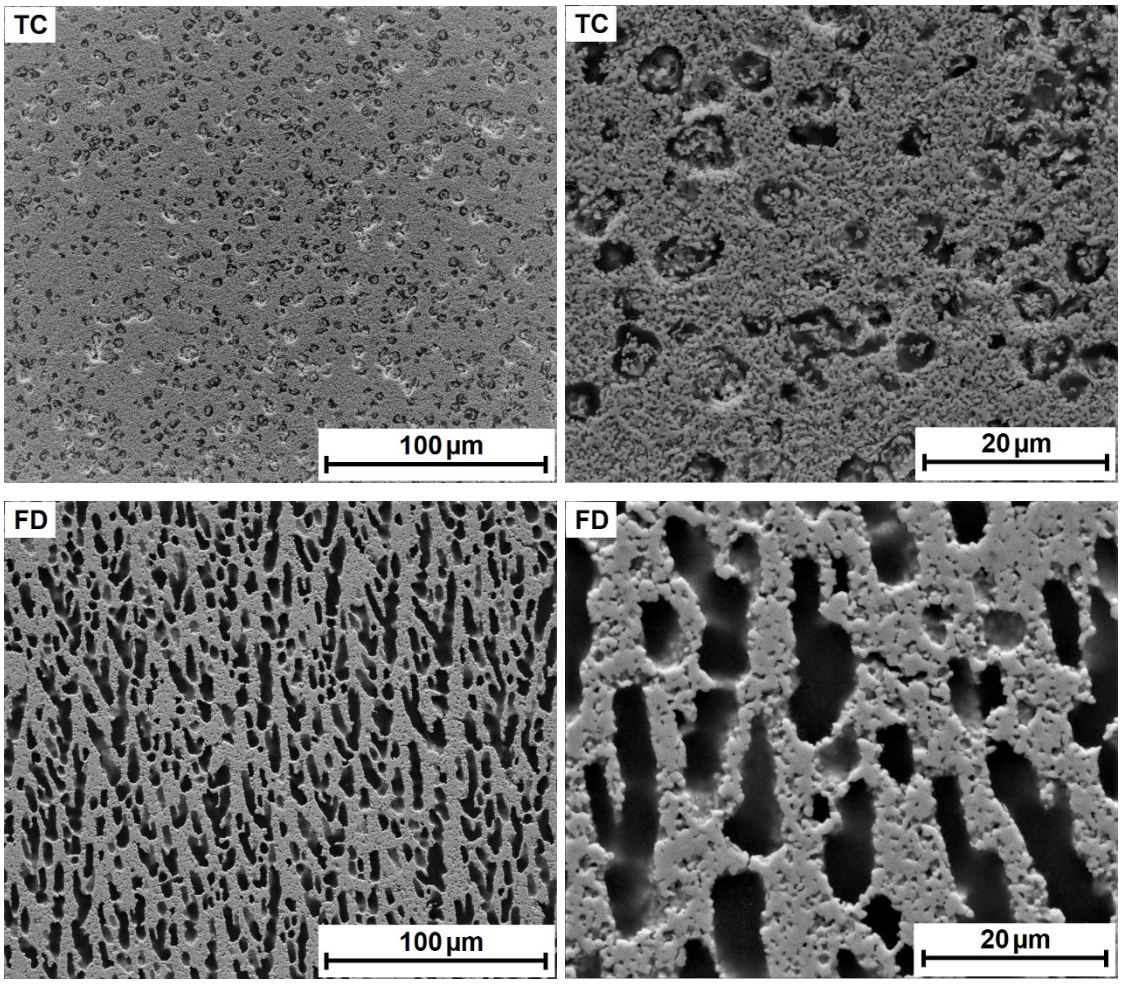

Figure 2 – Scanning electron microscopy cross section images of the porous 20GDC membranes produced by tape casting (top) and by freeze drying (bottom).

The sample produced by tape casting (Figure 2, top) has rounded pores of similar sizes, uniformly distributed after the removal of rice starch during the sintering stage. The FD sample (Figure 2, bottom) has a vertically aligned elongated pore structure, which is the replica of the original solvent crystals. The surfaces of freeze-dried samples were slightly sanded to remove irregularities caused at the air interface, and to eliminate small pores that are formed on the surface in contact with the metal base, which occurs due to nucleation of the ice crystals, as can be seen in Figure 3.

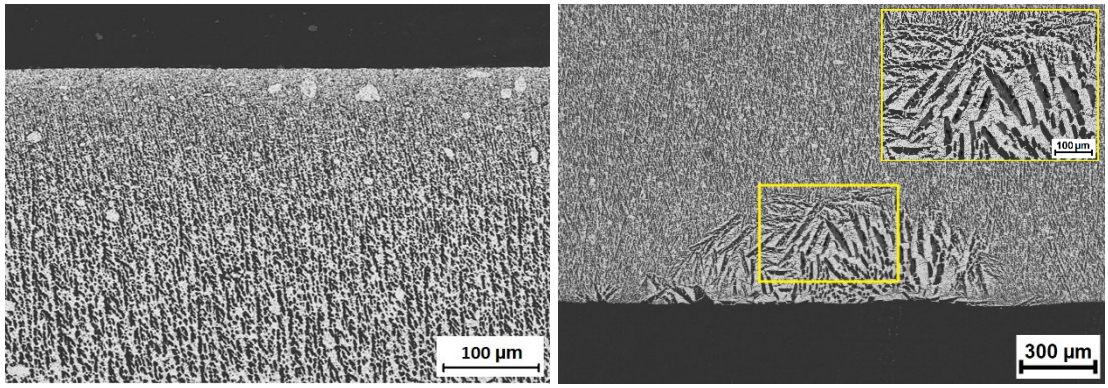

Figure 3 – Scanning electron microscopy cross section images of freeze-dried 20GDC samples. The image on the left shows the surface that was in contact with the metallic support; the one on the right shows the surface in contact with air during freezing. Direction of freezing: top to bottom.

After the preparation of the ceramic support, the porous membranes produced by tape casting had 0.6 mm thickness and 17 mm diameter, and by freeze drying 0.8 mm thickness and 23 mm diameter. These samples were infiltrated with molten carbonate at 600 ºC, and had their mass increased by approximately 130 mg for samples produced by tape casting, and 300 mg for the ones produced by freeze drying. Figure 4 shows images of the fractured surfaces of composite samples, to check if the filling process reached their bulk. Although polishing of the cross section had been carefully performed, there is evidence that part of the carbonate may have been lost during polishing. Thus, SEM images of the fractured membranes were used to verify the infiltration of carbonate, in addition to evaluation of the weight of the membrane before and after the infiltration process.

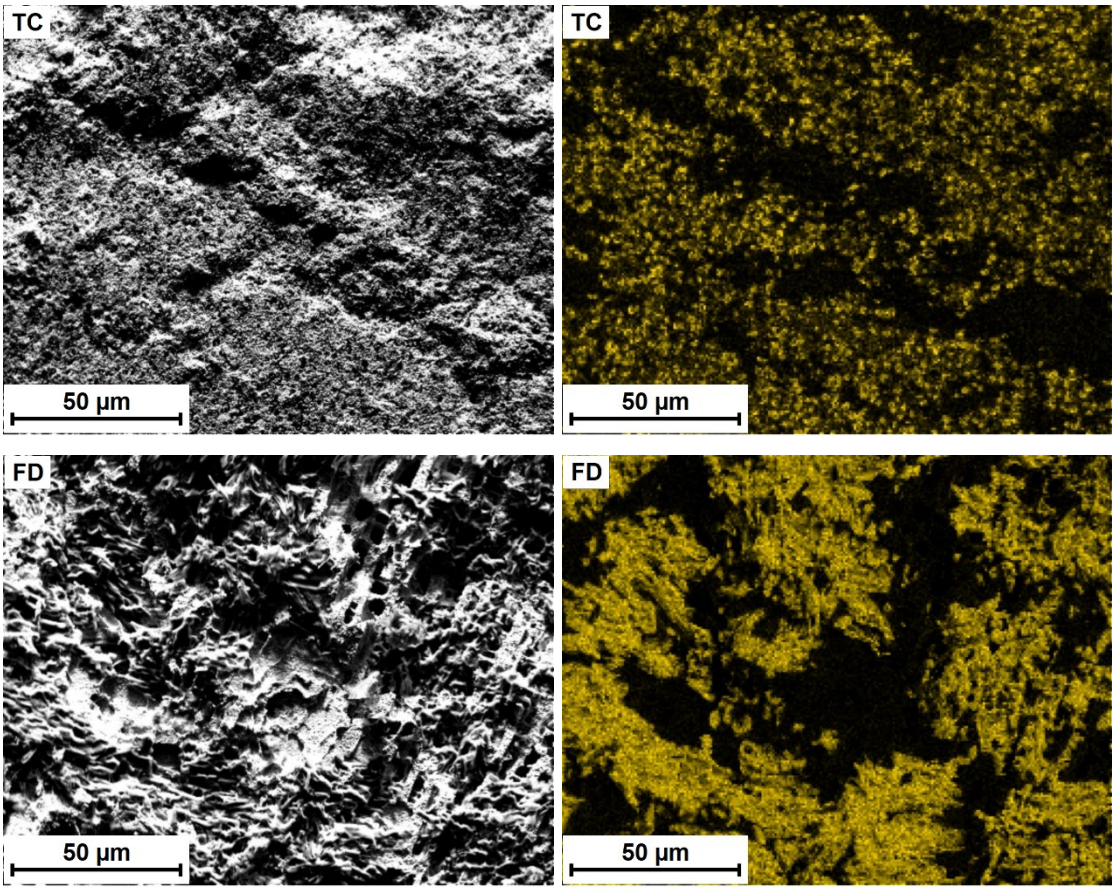

Figure 4 – SEM images of fracture surfaces of GDC membranes produced by tape casting (top) and freeze drying (bottom) with the corresponding sodium mapping (right) by EDS to verify carbonate infiltration.

The carbonate eutectic mixture had fully infiltrated into the membranes support, reaching their bulk (Figure 4). Since it was not a polished surface, the comparison of the amount of carbonate infiltrated into each type of microstructure was not possible in the micrographs; however, according to mass monitoring before and after the infiltration process, both samples had 40-45% of their volume filled by the eutectic carbonate composition. Values for open porosity and carbonate loadings are summarized in Table 1.

Table 1 – Open porosity and carbonate loadings, related to membrane total volume, for samples produced by tape casting and freeze drying.

Sample	Open porosity (%)	Carbonate loading	
		mass (mg)	vol.%
TC	47.1	130	43.3
FD	46.7	300	42.0

To ensure that the molten carbonate remained inside the membrane during the entire permeation test, SEM observations were performed in the bulk of a sample submitted to the same heat treatment. Figure 5 shows images of the membrane fracture surface before and after the heat treatment; a slight decrease in the amount of carbonate was detected inside the membrane, probably due to the reaction with the sealant, but sufficient retention of molten carbonate was detected.

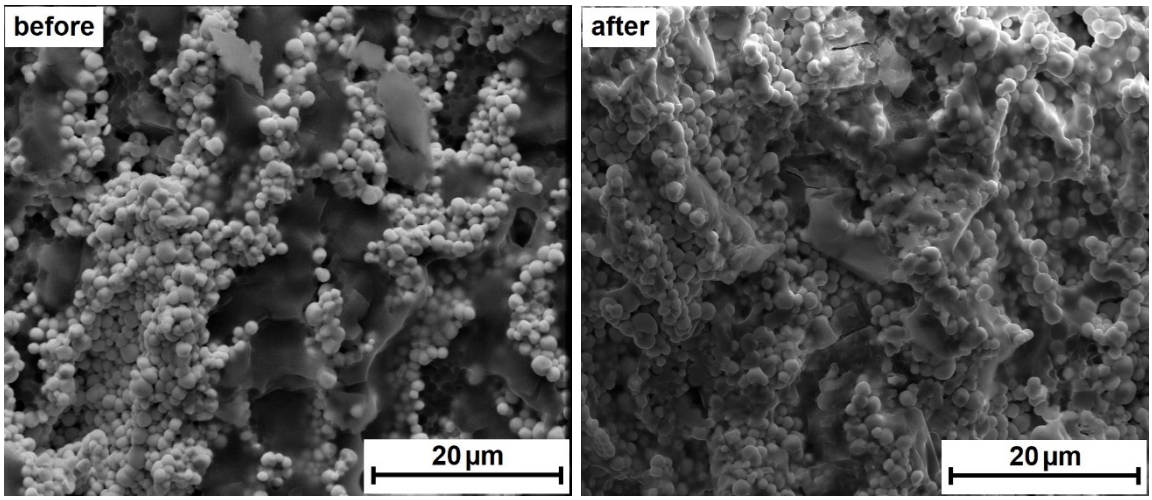

Figure 5 - SEM images of fracture surfaces of GDC membranes produced by freeze drying before (left) and after (right) permeation measurements.

To analyze the influence of the pore structure on the electrical resistivity of the final composite membrane, electrochemical impedance spectroscopy experiments were performed in membranes without and with carbonate infiltration. Figure 6 shows the impedance diagrams of the porous ceramic support at 580 °C in air, corrected for the sample dimensions.

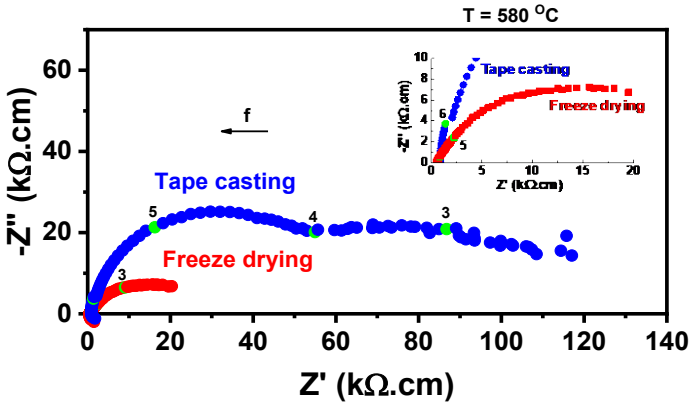

Figure 6 - Impedance spectroscopy diagrams of GDC porous samples produced by tape casting and freeze drying, sintered at 1450 °C. Temperature of measurement: 580 °C. Numbers stand for log f (f: Hz). Inset: zoom at the high frequency region.

At temperatures higher than 500 °C the bulk resistivity is not detected [34], but only the electrical contribution of the interfaces; the total (bulk and interfaces) electrical resistivity was evaluated at the intersection of the fitted diagram with the Z' axis in the low frequency region of the diagram. The total resistivity of TC and FD samples was 116.1 kΩ.cm and 25.5 kΩ.cm, respectively. The TC sample was considerably more resistive, and it is interesting to note that such difference in the electrical (ionic and electronic) resistivity is not related to porosity, once both samples have similar pore volume fractions (47%).

Porous ceramics have different electrical behavior from dense ceramics. Pores can be considered volume defects that prevent charge transport, acting as blockers to ion conduction [35-37]. The electric current lines, due to the application of an external electric field, can bypass the pores, producing a modification in the low-frequency region of the impedance diagrams of solid electrolytes (intergranular response). Similar behavior, i.e., the modification of the impedance diagram in the low-frequency region, has already been reported for the case of cracks in zirconia-based solid electrolytes [35] and in porous zirconia-yttria ceramics [38].

Considering that the samples were produced with the same ceramic material, sintered at the same temperature, and presented similar porosity values, the different values of electrical resistivity (Figure 6) is due to the difference of the pore structures. The sample with aligned porosity presents lower electrical resistivity in the

intergranular region due to the decrease in the average free path of charge carriers, i.e., due to the lower tortuosity along the electric field directions of the FD ceramic.

Figure 7 presents the impedance diagrams of ceramic-carbonate membranes produced by tape casting and freeze drying, measured at temperatures below and above the melting point of the sodium-lithium carbonate (500 ºC). The impedance diagrams can be described by the equivalent circuit of Figure 7c, which comprises two parallel paths, one representing the carbonate phase and the other the ceramic phase. The solid oxide path includes two series of a resistor (R) in parallel with a constant phase element (CPE), representing the contributions from the grain and the blocking region (grain boundary and pores), and the carbonate phase is represented by a single R//CPE [38,39]. At T < 500 ºC (Figure 7a), the electrical response of the composite is determined by the solid oxide phase. This behavior is due to the large difference of the electrical resistivity of the two phases. At higher temperatures higher than 500 ºC, the molten carbonate phase dominates the electrical response (Figure 7b), being the path that offers higher ionic transport, and indicates an effective percolation through the ceramic matrix. The semicircle at high frequency was not detected due to the contribution of the inductance of the coaxial cables of the impedance analyzer, and the observed impedance arc is ascribed to the electrodes. The impedance data were used to estimate the total resistivity of the membrane, determined at the intercept of the impedance diagram with the real axis in the high frequency region.

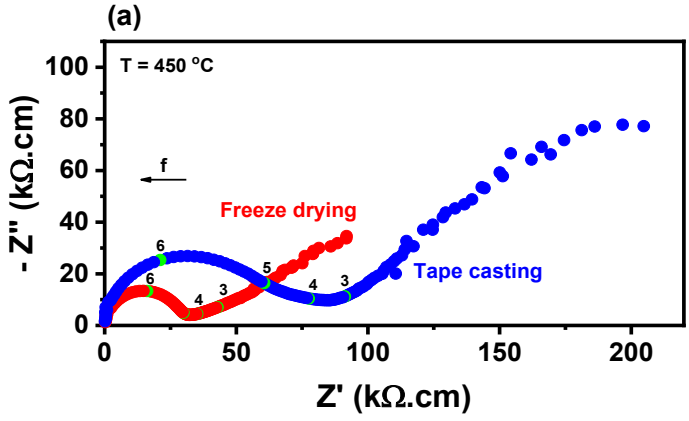

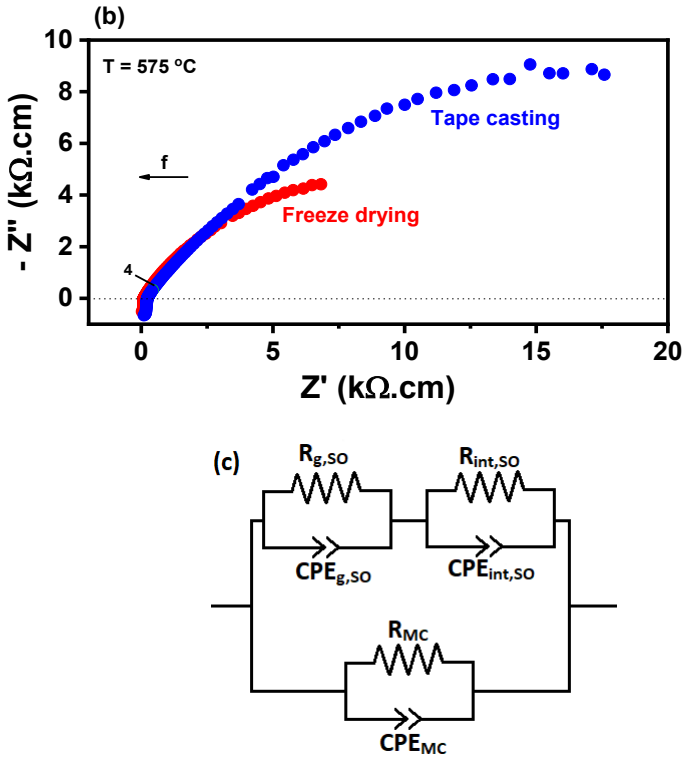

Figure 7 - Impedance spectroscopy diagrams of sodium-lithium carbonate infiltrated GDC-membranes produced by tape casting and freeze drying, sintered at 1450 °C, measured at (a) 450 °C and (b) 575 °C;(c) equivalent electrical circuit used to describe and analyze the data [40]. Numbers stand for log f (f: Hz)

Figure 8 shows Arrhenius plots of the total electrical conductivity of the ceramic-carbonate dual-phase membranes produced by tape casting and freeze drying, before and after the molten carbonate infiltration. The Arrhenius plots of the porous samples exhibit a linear behavior for the entire frequency range, as expected, with activation energy for oxide ion conduction of 82.0 kJ mol^{-1} and 91.7 kJ mol^{-1} for the tape cast and the freeze-dried ceramic support, respectively.

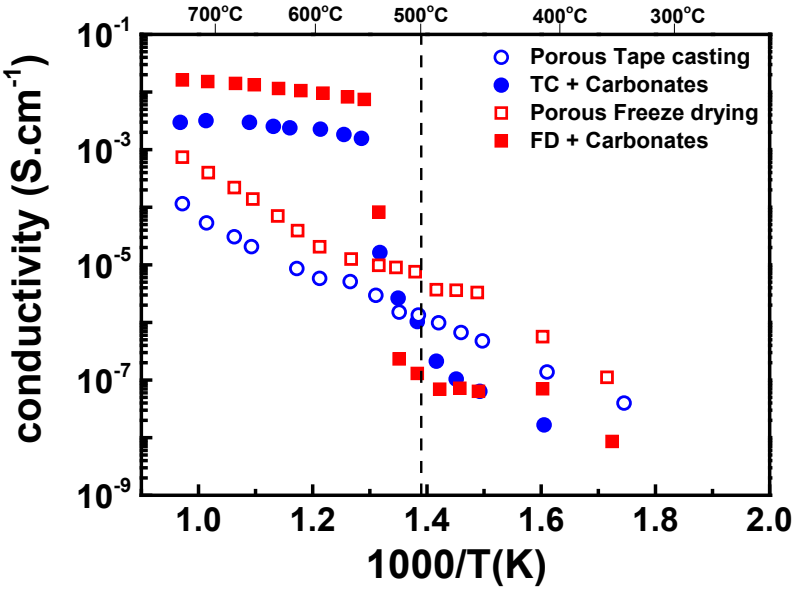

Figure 8- Arrhenius plots of the total electrical conductivity of porous GDC and sodium-lithium carbonate infiltrated GDC-membranes produced by tape casting and freeze drying.

The 20GDC ceramic membranes infiltrated with Na-Li molten carbonates show different dominant charge transport mechanisms, depending on the temperature range: lower than, near to and higher than ~ 500 ºC. At temperatures lower than 500 ºC the electrical conductivity of the membrane is basically due to oxygen ion conduction via the doped-ceria ceramic phase; close to 500 ºC the electrical conductivity increases steeply due to the contribution of the carbonate ion conduction, enhancing charge transport. During the transition to the contribution of the carbonate phase, the membrane conductivity increased by 4 to 5 orders of magnitude. In the upper temperature range the conductivity follows an Arrhenius behavior, dominated by the carbonate and alkali ions across the molten salt pathways. The evaluated activation energy for the high temperature regime is 24.1 kJ mol^{-1} for both samples, close to that reported for pure sodium-lithium carbonate eutectic mixture (~ 19.0 kJ mol^{-1}) [41].

The microstructure generated by the freeze-drying technique show higher electrical conductivity for both porous support and infiltrated membranes promoted their aligned pore structure, and consequently lower tortuosity across the transport pathway [42].

The performance of the CO_2 separation membrane was assessed by CO_2 permeation rate measurements, shown in Figure 9a. The temperature dependence of the permeation was measured during heating and cooling. At 800 ºC the CO_2 permeance was 5.35 x 10^{-7} mol m^{-2} s^{-1} Pa^{-1} and 3.44 x 10^{-7} mol m^{-2} s^{-1} Pa^{-1} during heating and cooling, respectively. That difference is probably due to the increased CO_2 leakage that occurred at temperatures above 850 ºC, produced by a slight reaction between the glue and the molten carbonate in the membrane; that reaction could increase the CO_2 concentration on the permeated side and decrease the CO_2 partial pressure, which is the driving force for the whole permeation process.

364

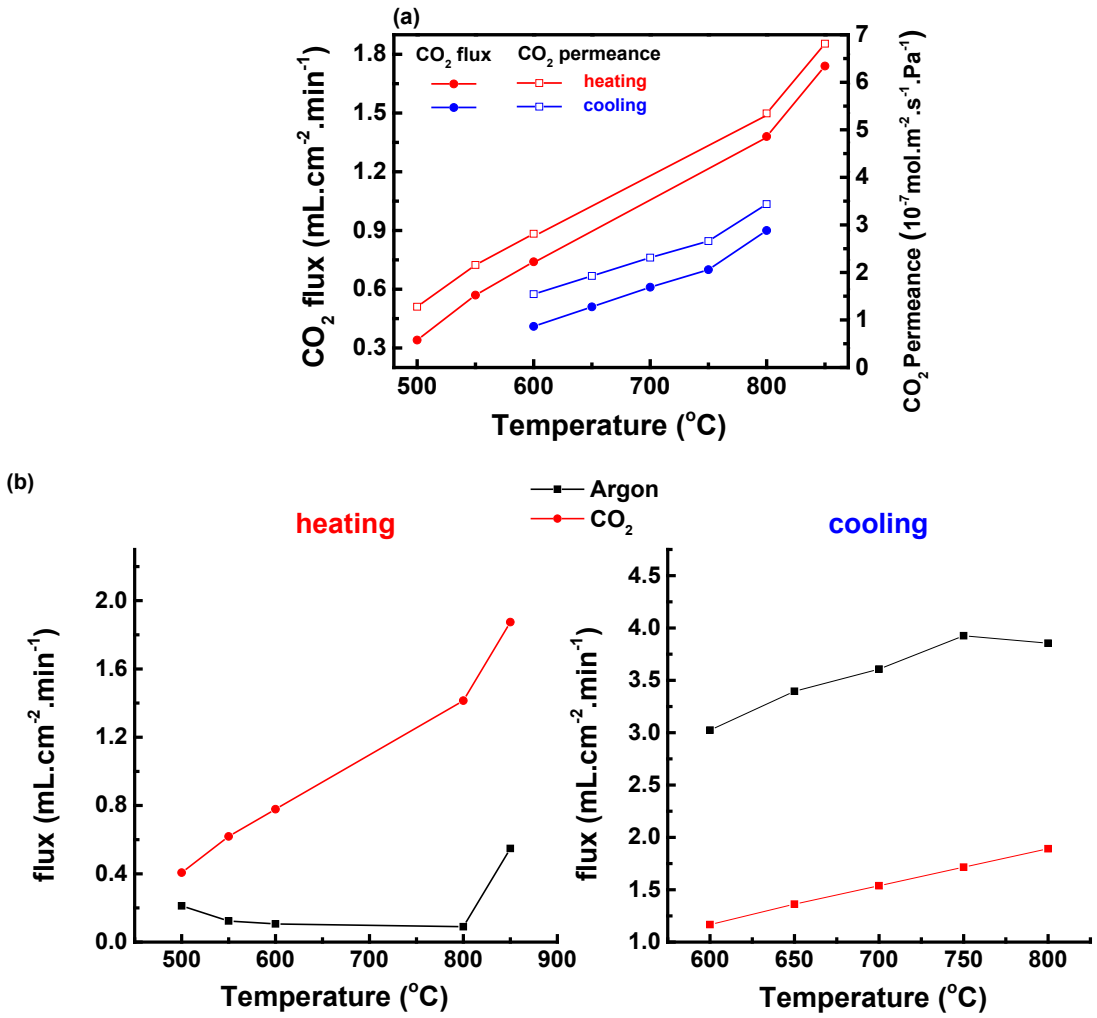

365

366

367

368 Figure 9 – (a) CO_2 flux permeation of dense dual-phase GDC membrane with freeze-
369 dried porous support and (b) Ar and CO_2 flux at permeated side, measured during
370 heating and cooling as a function of temperature; (c) Arrhenius plots of the CO_2
371 permeance.

Figure 10 shows the XRD pattern of the glue used to fix the membrane to the ceramic tube, measured after the permeation tests. In addition to sodium carbonate (Δ), the peaks (o) show the formation of $LiAlO_2$, evidencing the reaction of the molten carbonate with the sealant.

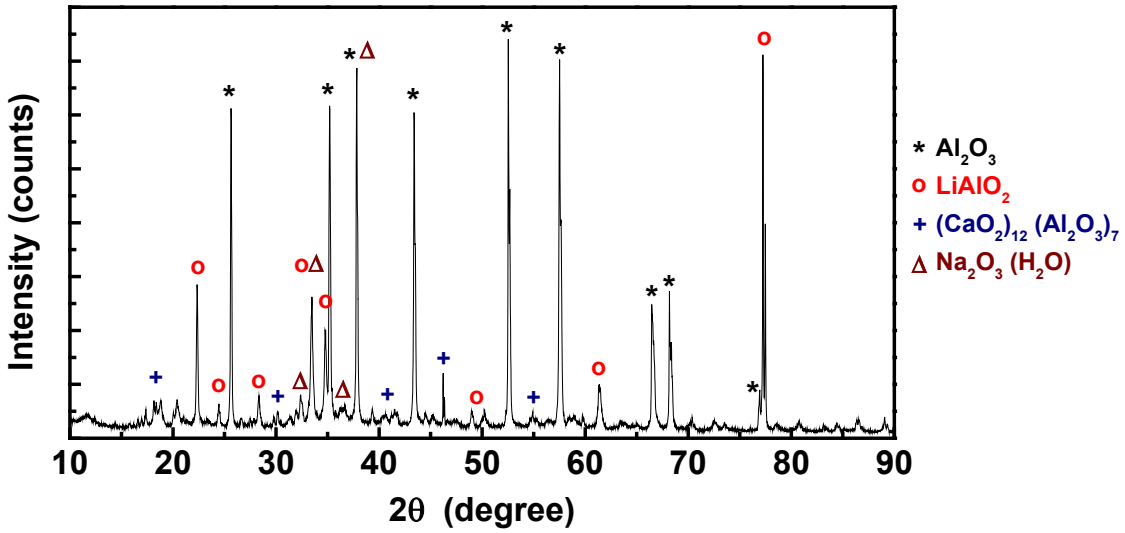

Figure 10 – Post-test XRD pattern of the glue used to fix the membrane during permeation tests.

The presence of sodium carbonate in the glue enables possible high temperature detachment of the membrane from the sealant, apparently leading to leakage.

Figure 9b shows the argon and carbon dioxide fluxes detected at the permeated side. Leakage control was performed by monitoring the amount of Ar detected and using the equations presented in section 2.3, the amount of CO_2 permeated was calculated excluding the leaked amount.

After the first heating and cooling cycle, depicted in Figure 9a, the membrane was kept at 600 ºC for over 30 h, then exhibiting stable CO_2 permeance of 1.5 10^{-7} mol m^{-2} s^{-1} Pa^{-1} (or CO_2 flux of 0.4 mL cm^{-2} min^{-1}).

The Arrhenius-type plots (Figure 9c) include the corresponding permeation activation energy (E_a) for the FD membrane, approximately 30 kJ mol^{-1}, a value between the activation energy of oxide-ion transport governed kinetics (70-80 kJ mol^{-1}) and the typical value found for molten alkali carbonates (approximately 20 kJ mol^{-1})

396 [42]. E_a indicates the energy required to initiate the permeation process,
397 characterized by the formation and transport of the carbonate ion. As the value lies
398 between the activation energy of the conduction process of O^{2-} and CO_3^{2-} ions, it is
399 an indication that the permeation is not limited either by the carbonate phase or by
400 the ceramic matrix, i.e., it is in a regime of mixed kinetic control.
401 Table 2 shows flux and CO_2 available permeation data, collected with ceramic
402 membranes having different ceramic matrices, geometries, and feed gas
403 compositions. Considering that the efficiency of the membrane depends on its
404 thickness and on gas composition of the feed and permeated sides, the permeation
405 data were compared considering the permeability of the membranes in each
406 experiment, taking into account the thickness and the CO_2 partial pressure driving
407 force. To make a better comparison, all results were evaluated for 600 ^oC,
408 considering the activation energy mentioned in each study.
409 The membranes produced by freeze drying, despite presenting the second
410 highest flux of CO_2, show the highest permeability value at 600 ^oC when temperature,
411 membrane thickness and CO_2 partial pressure are considered.
412
413

414 Table 2 – Collected CO_2 permeation data of several dual phase membranes

Ceramic matrix	Membrane geometry	Thickness (mm)	Feed gas	Temperature (°C)	CO_2 flux (mL/min cm^2)	Permeance (mol/m^2 s Pa)	Permeance at 600 °C (mol/m^2 s Pa)	Permeability at 600 °C (mol/m s Pa)	Reference
GDC	Disk	0.75	20%CO_2/15%H_2O/62.4%Ar/2.6% H_2	800 (heating)	1.380	5.35×10^{-7}	2.36×10^{-7}	1.77×10^{-10}	This work
				800 (cooling)	0.900	3.44×10^{-7}	1.56×10^{-7}	1.17×10^{-10}	This work
SDC	Hollow fiber	0.1	5%H_2/47.5%CO_2/47.5%N_2	700	5.460	8.56×10^{-7}	2.55×10^{-7}	2.55×10^{-11}	[25]
LSCF	Disk	0.375	50%CO_2/50%Ar	900	0.360	5.36×10^{-8}	2.26×10^{-9}	8.46×10^{-13}	[43]
BYS	Disk	0.05	50%CO_2/50%Ar	650	0.083	1.10×10^{-8}	4.73×10^{-9}	2.37×10^{-13}	[44]
SDC	Disk	0.8	10%H_2/45%CO_2/45%N_2	750	0.820	1.36×10^{-7}	3.65×10^{-8}	2.92×10^{-11}	[45]
SDC	Disk	1.5	50%CO/35%CO_2/10%H_2/5%N_2	900	0.790	1.68×10^{-7}	2.51×10^{-8}	3.76×10^{-11}	[46]
SDC-BYS	Tube	0.12	49.5%CO/36%CO_2/4.5%N_2/10%H_2	700	0.490	1.05×10^{-7}	4.40×10^{-8}	5.27×10^{-12}	[47]
GDC	Disk	0.92	50%N_2/50%CO_2	650	0.236	4.40×10^{-8}	3.08×10^{-8}	2.83×10^{-11}	[48]

4. Conclusions

Porous CeO_2: 20 mol% Gd_2O_3 oxide ion conductors prepared by tape casting and freeze-drying (FD) techniques, infiltrated with molten $(Na,Li)_2CO_3$ eutectic alkali carbonates, were successfully prepared. The side-to-side aligned porosity of GDC ceramic pellets prepared by the FD technique had a significant impact on the electrical properties of the composite membrane, producing membranes with improved electrical conductivity. The directional microstructure along the permeation axis favored the infiltration of a larger volume of carbonates, resulting in enhanced performance of the membrane for separation/capture of CO_2. The best value achieved for CO_2 permeance was 5.35 x 10^{-7} mol m^{-2} s^{-1} Pa^{-1} at 800 ^oC, higher than reported values. The main results showed that FD is a viable technique to scale up the production of efficient composite membrane for CO_2 separation/capture.

S.G.M. Carvalho: Conceptualization, Investigation, Data Collection, Methodology, Writing- Original draft preparation, **E.N.S. Muccillo**: Writing- Reviewing and Editing, **F.C. Fonseca**: Funding, Writing- Reviewing and Editing, **M. Müller**: Investigation, Writing- Reviewing and Editing, **F. Schulze-Küppers:** Data Collection, Investigation, **S. Baumann**: Writing- Reviewing and Editing, **W.A. Meulenberg**: Supervision, Funding, Methodology, Writing- Reviewing and Editing, **O. Guillon**: Funding, Writing- Reviewing and Editing, **R. Muccillo**: Supervision, Conceptualization, Methodology, Writing- Reviewing and Editing.

Funding: This work was supported by CNEN, CINE-SHELL (ANP) (FAPESP Proc. 2017/11937-4), CDMF-CEPID (FAPESP Proc. 2013/07296-2), and CNPq (Procs. 302357/2018-1, 305889/2018-4, and 305620/2019-3).

Acknowledgement: S.G.M.C. holds a post-doctoral fellowship provided by Shell under CINE-Shell (ANP) / FAPESP.

References

[1] S.K. Tandon, J. Mallik, Links between energy usage and climate: Implications on increasing CO_2 emissions and carbon capture and storage, Curr. Sci. 114 (2018) 1430–1437. https://doi.org/10.18520/cs/v114/i07/1430-1437.

[2] J.D. Figueroa, T. Fout, S. Plasynski, H. McIlvried, R.D. Srivastava, Advances in CO_2 capture technology-The U.S. Department of Energy's Carbon Sequestration Program, Int. J. Greenh. Gas Control 2 (2008) 9–20. https://doi.org/10.1016/S1750-5836(07)00094-1.

[3] E. Sanchez Fernandez, E.L.V. Goetheer, G. Manzolini, E. Macchi, S. Rezvani, T.J.H. Vlugt, Thermodynamic assessment of amine based CO_2 capture technologies in power plants based on European Benchmarking Task Force methodology, Fuel 129 (2014) 318–329. https://doi.org/10.1016/j.fuel.2014.03.042.

[4] N. Hüser, O. Schmitz, E.Y. Kenig, A comparative study of different amine-based solvents for CO_2-capture using the rate-based approach, Chem. Eng. Sci. 157 (2017) 221–231. https://doi.org/10.1016/j.ces.2016.06.027.

[5] T.C. Merkel, H. Lin, X. Wei, R. Baker, Power plant post-combustion carbon dioxide capture: An opportunity for membranes, J. Memb. Sci. 359 (2010) 126–139. https://doi.org/10.1016/j.memsci.2009.10.041.

[6] D. Shekhawat, D.R. Luebke, H.W. Pennline, A review of carbon dioxide selective membranes: A topological report, US DOE (2003) 9–11. http://www.fischer-tropsch.org/DOE/DOE_reports/NETL/2003-1200/NETL-2003-1200.pdf.

[7] E.J. Granite, T. O'Brien, Review of novel methods for carbon dioxide separation from flue and fuel gases, in Fuel Processing Technology 86 (2005) 1423–1434. https://doi.org/10.1016/j.fuproc.2005.01.001.

[8] M. Anderson, Y.S. Lin, Carbon dioxide separation and dry reforming of methane for synthesis of syngas by a dual-phase membrane reactor, AIChE J. 59 (2013) 2207–2218. https://doi.org/10.1002/aic.14103.

[9] J.A. Fabián-Anguiano, C.G. Mendoza-Serrato, C. Gómez-Yáñez, B. Zeifert, X. Ma, J. Ortiz-Landeros, Simultaneous CO_2 and O_2 separation coupled to oxy-dry reforming of CH_4 by means of a ceramic-carbonate membrane reactor for in situ syngas production, Chem. Eng. Sci. 210 (2019) 115250. https://doi.org/10.1016/j.ces.2019.115250.

[10] T. Chen, Z. Wang, L. Liu, S. Pati, M.H. Wai, S. Kawi, Coupling CO_2 separation with catalytic reverse water-gas shift reaction via ceramic-carbonate dual-phase

membrane reactor, Chem. Eng. J. 379 (2020) 122182.
https://doi.org/10.1016/j.cej.2019.122182.
[11] G.A. Mutch, L. Qu, G. Triantafyllou, W. Xing, M.L. Fontaine, and I.S. Metcalfe, Supported molten-salt membranes for carbon dioxide permeation, J. Mater. Chem. A 7 (2019) 12951–12973. https://doi.org/10.1039/c9ta01979k.
[12] S.J. Chung, J.H. Park, D. Li, J.I. Ida, I. Kumakiri, J.Y.S. Lin, Dual-phase metal-carbonate membrane for high-temperature carbon dioxide separation, Ind. Eng. Chem. Res. 44 (2005) 7999–8006. https://doi.org/10.1021/ie0503141.
[13] B. Lu, Y.S. Lin, Synthesis and characterization of thin ceramic-carbonate dual-phase membranes for carbon dioxide separation, J. Memb. Sci. 444 (2013) 402–411. https://doi.org/10.1016/j.memsci.2013.05.046.
[14] Z. Yang, Y. Zhu, M. Han, Synthesis and characterization of gadolinium doped ceria-carbonate dual-phase membranes for carbon dioxide separation, J. Alloys Compd. 723 (2017) 70–74. https://doi.org/10.1016/j.jallcom.2017.06.164.
[15] J.L. Wade, C. Lee, A.C. West, K.S. Lackner, Composite electrolyte membranes for high temperature CO_2 separation, J. Memb. Sci. 369 (2011) 20–29. https://doi.org/10.1016/j.memsci.2010.10.053.
[16] F.M.B. Marques, S.G. Patrício, E. Muccillo, R. Muccillo, On the model performance of composite CO_2 separation membranes, Electrochim. Acta 210 (2016) 87–95. https://doi.org/10.1016/j.electacta.2016.05.141.
[17] A. Gili, B. Bischoff, U. Simon, F. Schmidt, D. Kober, O. Görke, M.F. Bekheet, A. Gurlo, Ceria-based dual-phase membranes for high-temperature carbon dioxide separation: Effect of iron doping and pore generation with MgO template, Membranes (Basel). 9 (2019). https://doi.org/10.3390/membranes9090108.
[18] O. Ovalle-Encinia, P. Sánchez-Camacho, D. González-Varela, H. Pfeiffer, Development of New Bifunctional Dense Ceramic-Carbonate Membrane Reactors for Gas Mixtures Separation, through CO Oxidation and Subsequent CO_2 Permeation, ACS Appl. Energy Mater. 2 (2019) 1380–1387. https://doi.org/10.1021/acsaem.8b01947.
[19] S. Zhuang, N. Han, M. Xing, B. Meng, S. Liu, Perovskite oxide and carbonate composite membrane for carbon dioxide transport, Mater. Lett. 236 (2019) 329–333. https://doi.org/10.1016/j.matlet.2018.10.135.
[20] O. Ovalle-Encinia, H. Pfeiffer, J. Ortiz-Landeros, $Ce_{0.85}Sm_{0.15}O_{2-}$ $Sm_{0.6}Sr_{0.4}Al_{0.3}Fe_{0.7}O_3$ composite for the preparation of dense ceramic-carbonate

membranes for CO_2 separation, J. Memb. Sci. 547 (2018) 11–18. https://doi.org/10.1016/j.memsci.2017.10.021.
[21] O. Ovalle-Encinia, H. Pfeiffer, J. Ortiz-Landeros, CO_2 Separation Improvement Produced on a Ceramic-Carbonate Dense Membrane Superficially Modified with Au-Pd, Ind. Eng. Chem. Res. 57 (2018) 9261–9268. https://doi.org/10.1021/acs.iecr.8b01570.
[22] M. Kazakli, G.A. Mutch, G. Triantafyllou, A.G. Gil, T. Li, B. Wang, J.J. Bailey, D.J.L. Brett, P.R. Shearing, K. Li, I. Metcalfe, Controlling molten carbonate distribution in dual-phase molten salt-ceramic membranes to increase carbon dioxide permeation rates, J. Memb. Sci. 617 (2021) 118640. https://doi.org/10.1016/j.memsci.2020.118640.
[23] U. Gude, S. Baumann, W.A. Meulenberg, M. Müller, Towards the development of materials for chemically stable carbonate-ceramic membranes to be used for CO_2 separation in water-gas-shift reactors, Sep. Purif. Technol. 215 (2019) 378–383. https://doi.org/10.1016/j.seppur.2019.01.020.
[24] W. Xing, Z. Li, T. Peters, M.L. Fontaine, M. McCann, A. Evans, T. Norby, R. Bredesen, Improved CO_2 flux by dissolution of oxide ions into the molten carbonate phase of dual-phase CO_2 separation membranes, Sep. Purif. Technol. 212 (2019) 723–727. https://doi.org/10.1016/j.seppur.2018.11.090.
[25] T. Chen, Z. Wang, J. Hu, M.H. Wai, S. Kawi, Y.S. Lin, High CO_2 permeability of ceramic-carbonate dual-phase hollow fiber membrane at medium-high temperature, J. Memb. Sci. 597 (2020) 117770. https://doi.org/10.1016/j.memsci.2019.117770.
[26] L. Grima, G.A. Mutch, P.B. Oliete, W. Bucheli, R.I. Merino, E.I. Papaioannou, J.J. Bailey, M.D. Kok, D.J.L. Brett, P.R. Shearing, I.S. Metcalfe, M.L. Sanjuán, High CO_2 permeability in supported molten-salt membranes with highly dense and aligned pores produced by directional solidification, J. Memb. Sci. 630 (2021). https://doi.org/10.1016/j.memsci.2021.119057.
[27] A. Cordier, H. El Khal, E. Siebert, M.C. Steil, On the role of the pore morphology on the electrical conductivity of porous yttria-stabilized zirconia, J. Eur. Ceram. Soc. 39 (2019) 2518–2525. https://doi.org/10.1016/j.jeurceramsoc.2019.02.027.
[28] K.L. Scotti, D.C. Dunand, Freeze casting – A review of processing, microstructure and properties via the open data repository, FreezeCasting.net, Prog. Mater. Sci. 94 (2018) 243–305. https://doi.org/10.1016/j.pmatsci.2018.01.001.

548 [29] C. Gaudillere, J.M. Serra, Freeze-casting: Fabrication of highly porous and
549 hierarchical ceramic supports for energy applications, Bol. Soc. Esp. Ceram. V. 55
550 (2016) 45-54. https://doi.org/10.1016/j.bsecv.2016.02.002.
551 [30] L. Ren, Y.P. Zeng, D. Jiang, Fabrication of gradient pore TiO_2 sheets by a novel
552 freeze-tape-casting process, J. Am. Ceram. Soc. 90 (2007) 3001–3004.
553 https://doi.org/10.1111/j.1551-2916.2007.01833.x.
554 [31] S.W. Sofie, Fabrication of functionally graded and aligned porosity in thin
555 ceramic substrates with the novel freeze-tape-casting process, J. Am. Ceram. Soc.
556 90 (2007) 2024–2031. https://doi.org/10.1111/j.1551-2916.2007.01720.x.
557 [32] F. Schulze-Küppers, U.V. Unije, H. Blank, M. Balaguer, S. Baumann, R. Mücke,
558 W.A. Meulenberg, Comparison of freeze-dried and tape-cast support microstructure
559 on high-flux oxygen transport membrane performance, J. Memb. Sci. 564 (2018)
560 218–226. https://doi.org/10.1016/j.memsci.2018.07.028
561 [33] Image Processing and Analysis in Java. Available online: ttps://imagej.nih.gov/ij/
562 (accessed on 29 November 2021).
563 [34] R.K. Lenka, T. Mahata, A.K. Tyagi, P.K. Sinha, Influence of grain size on the
564 bulk and grain boundary ion conduction behavior in gadolinia-doped ceria, Solid
565 State Ionics 181 (2010) 262–267. https://doi.org/10.1016/j.ssi.2009.12.018.
566 [35] L. Dessemond, R. Muccillo, M. Hénault, M. Kleitz, Electric conduction-blocking
567 effects of voids and second phases in stabilized zirconia, Appl. Phys. A: Solids
568 Surfaces 57 (1993) 57–60. https://doi.org/10.1007/BF00331217.
569 [36] X. Guo, Physical origin of the intrinsic grain-boundary resistivity of stabilized-
570 zirconia: Role of the space-charge layers, Solid State Ionics 81 (1995) 235–242.
571 https://doi.org/10.1016/0167-2738(95)00180-E.
572 [37] M. Kleitz, L. Dessemond, M.C. Steil, Model for ion-blocking at internal interfaces
573 in zirconias, Solid State Ionics 75 (1995) 107–115.
574 https://doi.org/10.1016/0167-2738(94)00143-G.
575 [38] R. Muccillo, Impedance spectroscopy analysis of zirconia:8 mol% yttria solid
576 electrolytes with graphite pore former, J. Mater. Res. 24 (2009) 1780–1784.
577 https://doi.org/10.1557/jmr.2009.0209.
578 [39] S.G. Patrício, F.M.B. Marques, Benchmarking the ambipolar conductivity of
579 composite electrolytes for gas separation membranes, Int. J. Energy Res. 40 (2016)
580 2150–2161. https://doi.org/10.1002/er.3596.

[40] C.M. Soares, S.G. Patrício, F.M. Figueiredo, F.M.B. Marques, Relevance of the ceramic content on dual oxide and carbonate-ion transport in composite membranes, Int. J. Hydrogen Energy 39 (2013) 5424–5432. https://doi.org/10.1016/j.ijhydene.2013.12.121.

[41] T. Kojima, Y. Miyazaki, K. Nomura, K. Tanimoto, Electrical Conductivity of Molten Li_2CO_3–X_2CO_3 (X: Na, K, Rb, and Cs) and Na_2CO_3–Z_2CO_3 (Z: K, Rb, and Cs), J. Electrochem. Soc. 154 (2007) F222. https://doi.org/10.1149/1.2789389.

[42] Y. Shilong, Y. Zhupeng, L. Chuanming, C. Xiaowei, Z. Yanwei, Theoretical description on the interface-enhanced conductivity of SDC/LiNa-carbonate composite electrolytes, Mater. Lett. 92 (2013) 78–81. https://doi.org/10.1016/j.matlet.2012.10.062.

[43] M. Anderson, Y.S. Lin, Carbonate-ceramic dual-phase membrane for carbon dioxide separation, J. Memb. Sci. 357 (2010) 122–129. https://doi.org/10.1016/j.memsci.2010.04.009.

[44] Z. Rui, M. Anderson, Y. Li, Y.S. Lin, Ionic conducting ceramic and carbonate dual phase membranes for carbon dioxide separation, J. Memb. Sci. 417–418 (2012) 174–182. https://doi.org/10.1016/j.memsci.2012.06.030.

[45] T. Chen, H.C. Wu, Y. Li, Y.S. Lin, Poisoning Effect of H_2S on CO_2 Permeation of Samarium-Doped-Ceria/Carbonate Dual-Phase Membrane, Ind. Eng. Chem. Res. 56 (2017) 14662–14669. https://doi.org/10.1021/acs.iecr.7b03856.

[46] T.T. Norton, B. Lu, Y.S. Lin, Carbon dioxide permeation properties and stability of samarium-doped-ceria carbonate dual-phase membranes, J. Memb. Sci. 467 (2014) 244–252. https://doi.org/10.1016/j.memsci.2014.05.026.

[47] X. Dong, H.C. Wu, Y.S. Lin, CO_2 permeation through asymmetric thin tubular ceramic-carbonate dual-phase membranes, J. Memb. Sci. 564 (2018) 73–81. https://doi.org/10.1016/j.memsci.2018.07.012.

[48] S.G. Patrício, E. Papaioannou, G. Zhang, I.S. Metcalfe, F.M.B. Marques, High performance composite CO_2 separation membranes, J. Memb. Sci. 471 (2014) 211–218. https://doi.org/10.1016/j.memsci.2014.08.007.